



| | |
|--------------|---|
| Title | Isolated electrodeless high-frequency quartz crystal microbalance for immunosensors |
| Author(s) | Ogi, Hirotsugu; Motoshisa, Kazuma; Matsumoto, Takashi et al. |
| Citation | Analytical Chemistry. 2006, 78(19), p. 6903-6909 |
| Version Type | AM |
| URL | https://hdl.handle.net/11094/84136 |
| rights | This document is the Accepted Manuscript version of a Published Work that appeared in final form in Analytical Chemistry, © American Chemical Society after peer review and technical editing by the publisher. To access the final edited and published work see https://doi.org/10.1021/ac061004a . |
| Note | |

The University of Osaka Institutional Knowledge Archive : OUKA

<https://ir.library.osaka-u.ac.jp/>

The University of Osaka

Isolated Electrodeless High-Frequency Quartz Crystal Microbalance for Immunosensors

Hirotsugu Ogi, Kazuma Motoshisa, Takashi Matsumoto, Kenichi Hatanaka, and Masahiko Hirao

Graduate School of Engineering Science, Osaka University. Toyonaka, Osaka 560-8531, Japan

ogi@me.es.osaka-u.ac.jp

RECEIVED DATE

TITLE RUNNING HEAD: Isolated-Electrodeless QCM Biosensor

CORRESPONDING AUTHOR FOOTNOTE

Hirotsugu Ogi, Tel. +81-6+6850-6187, Fax: +81-6-6850-6187, E-mail: ogi@me.es.osaka-u.ac.jp

ABSTRACT

This paper presents a contactless technique to measure shear-bulk-wave resonance frequencies of an isolated quartz crystal in a flow cell. The line antenna placed outside the cell generates and detects the resonance frequencies in a wireless-electrodeless manner. It is revealed that this mechanism relies on the quasistatic electric field. A 0.3 mm thick AT-cut quartz was used and its overtone resonance frequencies up to 80 MHz were measured in liquids. Exact vibrational analysis was carried out for a triple-layered resonator system consisting of the adsorbed material layer, the electrode film, and the quartz plate. It predicts higher frequency sensitivity to the adsorbed material at higher modes when the electrode layer is removed. The 13th overtone (72-MHz resonance frequency) was used to detect human immunoglobulin G with concentrations between 0.1-20 $\mu\text{g/mL}$ captured by protein A immobilized on one side of the crystal. The real-time measurement of the frequency response yielded the equilibrium constant $K_A=5.21 \times 10^7 \text{ M}^{-1}$.

KEYWORDS Biosensors, Quartz crystal microbalance, wireless, electrodeless, IgG, Overtone

Piezoelectric crystals have been used to detect small amount of biochemical substances through their resonance-frequency changes; surface-modified crystals adsorb target substances, resulting in the increase of the effective mass¹ and the viscosity load^{2, 3}, and then in the decrease of the resonance frequencies. They made a real-time monitoring possible during antigen-antibody reactions and protein-ligand interactions without any labeling, providing their affinity and reaction rates. Quartz crystal microbalance (QCM) has been most intensively studied because of its high stability against the temperature change and pronounced coupling efficiency into the shear-vibrational modes in liquids. QCM is now recognized as a powerful tool for a biochemical sensor and served significant contributions to the study of various biochemical reactions, including immunoglobulins,⁴⁻⁹ DNAs,¹⁰⁻¹³ cocaine,¹⁴ and so on.

A wireless-electrodeless (contactless) isolated QCM technology will achieve important breakthrough for biochemical sensors, and this is significant challenge in this field because of three reasons. First, a metal-free oscillator will increase the amount of the frequency change to the adsorbed mass. Generally, metallic electrodes should be deposited on the oscillator surfaces for the excitation and detection of vibrations. The demand of decreasing the electric resistance has made the electrodes as thick as 100 nm or more. Attachment of such heavy electrodes, however, increases inertia resistance and also mechanical loss due to high damping of metals, deteriorating the sensitivity. (The Q values of metals are normally much lower than that of α -quartz. The Q value of a monocrystal copper is about 1000 near 1 MHz, for example.¹⁵) Although the use of higher frequencies (or thinner oscillators) causes larger frequency change when a material is adsorbed on the oscillator's surface,¹ the influence of the metallic electrodes enlarges as well at high frequencies, limiting the available frequency with QCM measurements. Thus, an electrodeless oscillator enhances the sensitivity, as will be shown analytically here. Second, we can study various coating materials for the oscillators, including nonconductive materials, when the restriction of the necessity of metallic electrodes is released. For example, a CVD diamond film can be a great candidate for the coating material because of its high affinity with human

body, extremely high stability owing to the covalent binding, and high corrosion resistance. Third, the wireless measurement allows us to perform an in-vivo experiment by isolating the oscillator, which will provide us with novel knowledge about the mechanism of antigen-antibody reactions.

The contactless acoustic measurements have been carried out by electromagnetic acoustic transducers (EMATs) for metallic or conductive materials.^{16, 17} An EMAT was composed of an rf coil and a magnet for making the coupling between the electromagnetic field and acoustic field owing to the Lorentz-force mechanism¹⁸ or the magnetostriction mechanism.¹⁹ The EMAT technology was successfully applied to piezoelectric materials, where the static magnetic field was dispensable because of the piezoelectricity: Johnson and Kim²⁰ studied the anelastic loss in langatate crystal using a free vibration of a cylindrical specimen excited by a surrounding solenoid coil. Ogi *et al.*^{21, 22} developed the electrodeless langasite oscillator using a solenoid-coil antenna. Concerning biochemical sensors, Thompson *et al.*²³ used the rf spiral coil located beneath an electrodeless quartz crystal and detected thickness-shear-mode resonance frequencies up to extremely high frequencies (~680 MHz). Vasilescu *et al.*²⁴ used the same technique for a GaPO₄ oscillator and suggested the great potential of the contactless oscillator as a biosensor. Thompson *et al.*²³ analyzed the coupling mechanism between the electromagnetic and the acoustic fields, considering the rotational component of the electric field as the principal cause, although it cannot explain observations as shown in this study. Therefore, the coupling mechanism for the electrodeless piezoelectric oscillator remains unclear.

For the further advancement, the sensor coil should be placed outside the QCM cell to carry out an isolated QCM system. However, the electrodeless coupling method using the spiral coil allowed an air gap as small as 30 μm ,²³ making the isolation of the crystal very difficult. Thus, an isolated QCM system has not been achieved. (We recently developed an isolated nickel oscillator using a piezomagnetic effect.²⁵)

We here present the isolated wireless-electrodeless QCM as a biochemical sensor. The noncontacting measurement of the resonance frequency is made possible by the line antenna placed outside the QCM cell, which generates and detects vibrations of the crystal with an air gap larger than 3

mm. The resonance frequency is detected up to 80 MHz in water. First, we investigate the coupling mechanism for the electroless measurement using an α -TeO₂ crystal. Second, we analyze the effect of the elastic coupling between the base crystal and the attached substance to evaluate the effect of the electrode layer on the sensitivity. Third, we develop a homebuilt QCM system and apply it to detect human immunoglobulin G (IgG) captured by protein A immobilized on the crystal surface in a flow-cell system. They are uniquely combined with each other through high affinity between the Fc fragment of IgG and protein A.²⁶⁻²⁸

COUPLING MECHANISM

Based on the EMAT technology, the coupling mechanism between the electromagnetic field radiated from an rf coil element and the acoustic vibrations in a piezoelectric material was considered. Thompson *et al.*²³ analyzed the phenomena, considering that the coupling was caused by the rotational component of the electric field \mathbf{E}_ω , which is expressed by $\mathbf{E}_\omega = -\partial\mathbf{B}/\partial t$ with the magnetic flux density \mathbf{B} . We, however, indicated that the coupling mechanism relies rather on the non-rotational component or the quasistatic electric field \mathbf{E}_{qs} (i.e. $\mathbf{E}_{qs} = -\text{grad}\phi$, where ϕ denotes the electric potential), than \mathbf{E}_ω .²² Here, we clarify the principal mechanism using an α -TeO₂ plate, which shows tetragonal symmetry and possesses only one independent piezoelectric coefficient,²⁹ making it easier to identify the mechanism. Figure 1 shows the specimen plate we used. The x' , y' , and z' axes are set along the $\langle 110 \rangle$, $\langle 1\bar{1}0 \rangle$, and $\langle 001 \rangle$ directions of the crystal. The dimensions are 0.318 mm (thickness), 7 mm, and 5 mm along the x' , y' , and z' axes, respectively. In this coordinate system, the piezoelectric coefficient matrix takes the form

$$[e'_{ij}] = \begin{bmatrix} 0 & 0 & 0 & e'_{14} & 0 & 0 \\ 0 & 0 & 0 & 0 & -e'_{14} & 0 \\ 0 & 0 & 0 & 0 & 0 & 0 \end{bmatrix}. \quad (1)$$

Here, $e'_{14}=0.330 \text{ C/m}^2$. Equation (1) indicates that no coupling occurs between the electric and acoustic fields with the electric field along the z' axis ($\langle 001 \rangle$ direction) because $e'_{3i}=0$, and that the shear wave polarized in the z' direction will be generated in the x' direction by the electric field along the y' axis. Therefore, by placing the α -TeO₂ plate on an elongated spiral coil, we can identify the dominant factor for the coupling (either \mathbf{E}_ω or \mathbf{E}_{qs}), because \mathbf{E}_ω appears along the rf current, whereas the direction of \mathbf{E}_{qs} is principally perpendicular to the current direction.

Figure 2 shows the resonance spectra measured using the elongated spiral coil with the two measurement setups. (The details to obtain the spectra will be shown later.) In the measurement setup in Fig. 2(a), the direction of \mathbf{E}_ω is parallel to the $\langle 001 \rangle$ direction, and no acoustic resonance would have been caused if the rotational electric field had been the principal factor. However, we clearly see the resonance peaks of the 1st, 3rd, and 5th overtones. (Using the reported elastic constants and the mass density, we calculated the fundamental resonance frequency to be 3.32 MHz, which agreed with the measured value of 3.36 MHz.) On the other hand, the measurement setup in Fig. 2(b) caused no resonance peaks, regardless of the parallel direction of \mathbf{E}_ω to $\langle 110 \rangle$. Considering \mathbf{E}_{qs} as the dominant factor, however, these observations can be explained consistently. Therefore, the quasistatic electric field must be the dominant factor for the electrodeless piezoelectric oscillators, not the rotational field.

Figure 3 shows the resonance spectra of the same α -TeO₂ plate measured by the line antenna, which we use in the following QCM study. In this case, only the quasistatic electric field appears along the direction perpendicular to the straight-line parts of the antenna. The results agree well with those observed by the elongated spiral coil in Fig. 2. Furthermore, the resonance-peak height increased by a factor of 5, indicating higher coupling efficiency with this configuration.

We note that both spiral coil and line antenna detected the resonance frequencies only of odd-number overtones. This is explained as follows: The quasistatic electric field radiated from the antenna or the coil penetrates throughout the thickness of the oscillator and the polarization of the electric field is uniform in the oscillator. Even-number overtone modes cause opposite signs of the shear strain near the both surfaces as illustrated in Fig. 4(a). Therefore, they require opposite polarization directions of

the electric field on the two sides. On the other hand, odd-number overtone modes cause the shear strain of the same sign near the both sides and the same polarization direction of the electric field can generate them (Fig. 4(b)).

Therefore, these observations strongly support our view that the electrodeless piezoelectric oscillator is driven by the quasistatic electric field.

VIBRATIONAL ANALYSIS

Conventional Sauerbrey equation¹ estimates the amount of the adsorbed substance on oscillator's surface from the frequency change Δf via:

$$\Delta f = -nf_1 \frac{\rho_s}{\rho_{osc} d_{osc}} . \quad (2)$$

ρ_{osc} and d_{osc} denote the mass density and the thickness of the oscillator, respectively; and ρ_s denotes the area mass density (mass/area) of the adsorbed material layer. f_1 is the fundamental resonance frequency before the adsorption reaction and n denotes the overtone number. Thus, the classical Sauerbrey equation predicts the linear dependence of the frequency change Δf on the fundamental frequency f_1 with the proportionality constant of the ratio between the adsorbed mass and the oscillator mass. Viscosity and mass of surrounding liquid also contribute to the decrease the resonance frequency and their influence has been estimated through the square-root dependence of the frequency:^{2,3}

$$\Delta f = -\sqrt{nf_1} \frac{1}{\rho_{osc} d_{osc}} \sqrt{\frac{\rho_l \eta_l}{4\pi}} . \quad (3)$$

Here, ρ_l and η_l are the mass density and the shear viscosity of the surrounding liquid. Thus, the use of a higher overtone mode leads to larger frequency shift for the mass of the adsorbed molecules while the viscosity effect becomes less significant compared with the mass effect. This function serves to avoid overestimating the amount of the adsorbed material.

When the elastic coupling occurs between the oscillator and the adsorbed substance layer, the strain energy arises in the substance layer and causes the additional frequency decrease. Few studies discussed this effect whereas it becomes significant at higher frequencies for softer layers, as shown later. We investigate the effect of the elastic coupling on the frequency shift assuming an IgG film on a quartz crystal plate, and also the effect of the electrode layer (when used) on the sensitivity.

For this, we analyze the frequency equation for a triple-layered resonator:

$$G_3 k_3 \tan p = G_2 k_2 \tan(\gamma - \delta) , \quad (4)$$

where,

$$\left. \begin{aligned} \cos \delta &= \cos \alpha \cos \beta + \kappa \sin \alpha \sin \beta \\ \sin \delta &= \cos \alpha \sin \beta - \kappa \sin \alpha \cos \beta \end{aligned} \right\} , \quad (5)$$

and

$$\begin{aligned} \alpha &= k_1 d_1, \quad \beta = k_2 d_1, \quad \gamma = k_2 (d_1 + d_2), \\ p &= k_3 d_3, \text{ and } \kappa = \frac{G_1 k_1}{G_2 k_2}. \end{aligned} \quad (6)$$

G_i , d_i , and k_i denote the shear modulus, the thickness, and the wavenumber in the i th layer, respectively ($i=1, 2, 3$). k_i is expressed by the resonance frequency f , the mass density ρ_i , and the shear modulus G_i as $k_i = 2\pi f \sqrt{\rho_i / G_i}$. Equation (4) was derived by considering six element plane (shear) waves, which travel upward and downward in the thickness direction, experiencing reflection and transmission at the interfaces.³⁰ It applies also to a double-layered system by taking $d_3=0$, for example.

EXPERIMENTAL SECTION

Isolated QCM. Figure 5 shows our homebuilt QCM cell. An AT-cut quartz oscillator with $5 \times 4 \text{ mm}^2$ area and 0.31-mm thickness is placed inside the acrylic cell. The thickness direction is along crystal's Y' direction. The line antenna is set outside the cell, making the QCM isolated completely. The antenna consists of three straight wires, two for generation and detection of the through-thickness resonance vibrations, and the other for grounding. When a sinusoidal voltage is applied to the

generation wire, the quasistatic electric field E_z occurs in the Z axis of the crystal, being parallel to the surface. This field generates plane waves propagating in the thickness direction through the converse piezoelectric effect. After the excitation, the detection wire detects the crystal's vibrations through the piezoelectric effect. The received signals enter the superheterodyne spectrometer to extract the same frequency component as the driving signal.¹⁷ A frequency scan yields the resonance spectrum and the Lorentzian-function fitting provides the resonance frequencies.

Surface Preparations. We tried two kinds of surface modifications. First was the silane-binding method following Muramatsu *et al.*⁴ A 10 nm Pt thin film was deposited on one side of the oscillator by the magnetron sputtering method after the physical etching of that surface. (The Pt film was needed for making the silane binding effective, not for an electrode.) The oscillator was cleaned in the piranha solution (98% H_2SO_4 :33% H_2O_2 =4:1). After rinsing with ultrapure water, it was immersed in a 5% γ -aminopropyl triethoxysilane for 24 h, rinsed with acetone, and dried in a vacuum. It was immersed in a 0.05 M glutaraldehyde solution for 3 h and ablated by 0.05-M phosphate-buffer solution (PBS, pH 7.0). Protein A was then immobilized on the surface by immersing the oscillator into the PBS containing 1 mg/ml protein A for 24 h at 4 °C. The remaining unreacted aldehyde was blocked with a 0.1 M glycine solution.

The second surface modification method was the gold-thiol modification. A 9 nm thick Au film was deposited after 1 nm Cr film on one side of the crystal. After cleaning by the piranha solution and rising ultrapure water, the crystal was immersed in 50 μ M 5-carboxy-1-pentanethiol/ethanol solution for 3 h. The surface was activated by 100 mM EDC (1-ethyl-3-(3-dimethylaminopropyl)carbodiimide, hydrochloride) solution and 100 mM sulfo-NHS (N-hydroxysulfosuccinimide sodium salt) solutions. Protein A was immobilized and the remaining activated ester sites were blocked by the glycine solution with the same procedure as the silane-binding method.

Human IgG was obtained from Athens Research and Technology, Inc. (product num. 16-16-090707; purity \geq 95%). Protein A was obtained from Zymed Laboratories, Inc. (product num. 10-

1100; purity 98%). 5-carboxy-1-pentanethiol (product num. C387) and EDC (product num. W001) were obtained from Dojindo Laboratories. Sulfo-NHS was purchased from Sigma-Aldrich Japan (product num. 56485). All of other chemical substances were purchased from Wako Pure Chemical Industries Ltd.

Flow-Cell System. The isolated QCM cell is installed into the homebuilt flow system as shown in Fig. 6. The temperature of the QCM cell was kept constant at 37 ± 0.02 °C. PBS steadily flows as a carrier fluid with a flow rate between 0.3-0.6 mL/min. We monitored the resonance frequency of the 13th overtone mode near 71.7 MHz. After the resonance frequency became stable, the IgG solution (PBS containing small amount of IgG) was injected. Glycine-HCl buffer (0.1 M, pH 2.2) was then injected for dissociating IgG molecules from protein A, which was followed by the injection of the carrier PBS. This sequence (PBS, IgG, Glycine-HCl, PBS, ...) was repeated with various IgG concentrations between 0.1 and 20 $\mu\text{g/mL}$.

RESULTS AND DISCUSSION

Resonance Spectrum. Figure 7 shows the typical resonance spectra measured in air and in water. According to Christoffel's equation,³¹ the electric field radiated from the antenna causes three bulk waves: the pure shear wave polarized in the X axis, the quasi-shear wave principally polarized in the Z' axis, and the quasi-longitudinal wave, all traveling in the thickness direction (Y' direction). We calculated their fundamental resonance frequencies using the reported values of the elastic constants and mass density of α -quartz.³¹ The results are $f_s^1=5.516$, $f_{qs}^1=6.310$, and $f_{ql}^1=11.71$ MHz, respectively, showing good agreement with measurements in Fig. 7. Because the quasi-shear wave and quasi-longitudinal wave have the out-of-plane displacements, they fail to resonate in water due to the energy

leakage. However, the pure shear-wave resonance occurs in water up to 80 MHz, which is the upper frequency limit of our generator. As expected, only the odd-number overtone modes were detected.

Elastic-Coupling Effect on the Frequency Shift. Figure 8 shows the fractional frequency change, $\Delta f/f$, calculated from Eq. (4) for the double-layer plate consisting of an AT-cut quartz and an IgG layer on it ($f=nf_1$). We used $G_{osc}=29$ GPa, $\rho_{ocs}=2469$ kg/m³, and $d_{osc}=0.3$ mm, standard values for an AT-cut quartz. Parameters used for the IgG layer were $\rho_{IgG}=1500$ kg/m³ and $d_{IgG}=20$ nm. We assumed various values for the shear modulus, G_{IgG} , of the IgG layer. The viscosity effect was not included.

When G_{IgG} is large, $\Delta f/f$ does not depend on the overtone number and it agrees with the prediction by the Sauerbrey equation (dashed line in Fig. 8(a)). A larger modulus corresponds to a longer wavelength and causes negligible shear strain in the IgG layer because of the free surface there. Thus, this case corresponds to the addition of the layer mass on the oscillator surface, and $\Delta f/f$ is independent of the overtone number, causing no elastic coupling. On the other hand, as G_{IgG} becomes smaller, the shear wave tends to produce larger shear strain in the IgG layer, and the resonance frequency of the system decreases. This trend can be remarkable for higher frequencies or shorter wavelengths. It is not straightforward to estimate the shear modulus of the IgG layer, but, if there is any elastic interaction between the IgG and the oscillator, we expect higher sensitivity to the adsorption for higher overtone resonance modes. We note that $\Delta f/f$ shows a linear dependence on the mass of the adsorbed material even when the elastic coupling occurs as shown in Fig. 8(b), indicating that we can evaluate kinetic constants from the time-decay behavior of the frequency as discussed below.

Figure 9 demonstrates the effect of the electrode on the frequency sensitivity. The calculation was made for a typical case; the triple-layer plate consisting of a 0.3 mm AT-cut quartz, 250 nm Au electrode (one side), and 20 nm IgG layer in this order. When the Au electrode is deposited on one side

of the oscillator, $\Delta f/f$ decreases in magnitude. This effect becomes more remarkable as the frequency increases.

Therefore, the use of higher frequencies and the exception of the metallic layer should be advantageous for the detection of biochemical substances.

Kinetic Analysis. Figures 10 shows the typical response of the resonance frequency during the injection sequence. We observed the identical frequency response between the two surface modification methods as shown in Fig. 11. The amount of the frequency change caused by the IgG adsorption increased with the increase of the IgG concentration, and the frequency change obeyed the exponential-decay law as shown in Figs. 12 and 13(a).

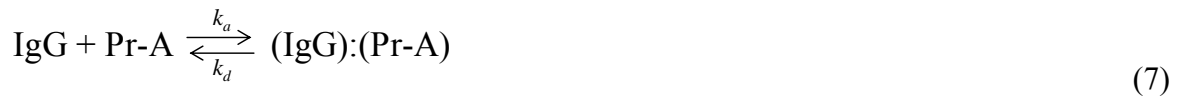
The glycine-HCl solution remarkably increased the resonance frequency, over the baseline level (Fig. 10). One reason is the dissociation of IgG molecules and the other is the difference of the dielectric constant of the glycine HCl solution. The injection of PBS after glycine-HCl caused a spike in the resonance frequency, and then decreased the frequency to the baseline level. The resonance frequency of the electrodeless QCM is thus affected by the surrounding liquids, because the naked surface allows the electrical coupling between the crystal and the surrounding fluid. (In other words, it can be a dielectric sensor.) However, because we used the frequency response in the same surrounding liquid for the following analysis, this effect is not included in the resultant kinetic constants.

The real-time measurement was continuously done for more than 24 h (more than 12 sequences) and reproducibility of these observations was well confirmed. Thus, our isolated QCM system well works as an immunosensors.

First, we compare the amount of the frequency shift observed here with those reported with conventional QCMs. To discuss the mechanical sensitivity of a QCM, it is reasonable to evaluate the frequency change standardized by the loaded mass, the measuring frequency, and crystal's mass.

Therefore, the area-mass density ρ_s in Eq. (2) can be the measure for this evaluation. Table 1 compares quantities observed by our QCM with those reported by conventional QCMs for the nearly same IgG concentration. We note that the standardized frequency change (sensitivity) in our QCM is larger than that of Muramatsu *et al.*⁴ regardless of less contribution of the viscosity effect due to high frequencies and of the same binding system (IgG-protein A). Thus, our QCM shows comparable or higher frequency change to the loaded mass compared with conventional QCMs.

Next, we analyze the frequency response to discuss the kinetics of the binding reaction between IgG and protein A (Pr-A) shown by



Such a binding reaction is usually characterized by three kinetic constants; the association rate constant k_a , the dissociation rate constant k_d , and the equilibrium constant K_A given by

$$K_A = \frac{k_a}{k_d}. \quad (8)$$

These quantities inform us of thermodynamic binding behavior at the equilibrium condition and average kinetics of molecules during association and dissociation processes. The real-time frequency measurement during the binding process allows us to determine these constants when three assumptions are made:^{6, 7, 32}

- (i) The binding reaction occurs with a pseudo-first-order manner.
- (ii) Concentration of IgG is constant throughout the reaction.
- (iii) $\Delta f/f$ is proportional to the amount of the adsorbed IgG molecules on protein A.

The exponential decay during the binding reaction (Figs. 11 and 12) accepts the first assumption. The second assumption will be acceptable when we use a flow cell system, where the IgG is continuously supplied. However, the IgG concentration in the QCM cell increases until it reaches the saturation value. The volume of the cell is 160 mm^3 and we expect 20 s to reach the saturation. Therefore, we did not use the frequency data for 150 s from the beginning of the binding reaction for determining the exponential coefficient. The calculation result in Fig. 8(b) verifies the third assumption even if the elastic coupling occurs.

Several researchers discussed the relationship between the frequency change and the kinetics of the binding reaction based on the assumptions and derived formulas given by^{6, 33}

$$\frac{\Delta f(t)}{f_0} = \text{const.} \left[e^{-(k_a C_{\text{IgG}} + k_d)t} - 1 \right], \quad (9)$$

$$\frac{1}{\Delta f_e} = \frac{1}{\Delta f_{\text{max}}} + \frac{1}{\Delta f_{\text{max}} K_A} \cdot \frac{1}{C_{\text{IgG}}} \quad (10)$$

Hence, $\Delta f(t) = f_0 - f(t)$ denotes the amount of the frequency change from the frequency value just before the reaction, f_0 . Δf_e is the frequency change at the equilibrium state, Δf_{max} denotes the possible maximum frequency change which would occur when all the immobilized protein-A molecules were bound with IgG. C_{IgG} denotes the IgG concentration in the QCM cell. Thus, plotting $1/C_{\text{IgG}}$ versus $1/\Delta f_e$ yields a line, whose slope and intercept equal $1/(\Delta f_{\text{max}} K_A)$ and $1/\Delta f_{\text{max}}$, respectively. Figure 13(b) shows such a plot.

Equation (9) predicts that the frequency decays exponentially with time and fitting an exponential function yields $k_a C_{\text{IgG}} + k_d$. We used measurements for highest-concentration IgG solutions in this procedure because of their better signal-to-noise ratio.

We then determine all the three constants by measuring Δf_e with various IgG concentrations and the dynamic response of the resonance frequency. Table 2 shows the results together with reported values.

Equilibrium constant K_A for IgG-protein A system is much higher than those for other systems, indicating high affinity between the IgG-Fc and protein A. The present value is larger than that reported previously by the SAW method³⁴ and closer to the values of the IgG-protein A binding in their solution phases (10^6 - 10^{10} M⁻¹)²⁸.

CONCLUSION

Contactless measurement of resonance frequencies of an isolated AT-cut quartz crystal was achieved by the line antenna placed near the crystal with a gap. The proposed method did not require electrodes on the crystal's surface and made it possible to isolate the oscillator completely.

The electrodeless measurements for the α -TeO₂ crystal revealed that the coupling between the electric and acoustic fields was caused by the quasistatic electric field, not by the rotational component of the electric field.

The vibrational analysis was analyzed for a triple-layered plate and it indicated higher sensitivity at higher overtone modes because of the elastic coupling between the oscillator and adsorbed material. Also, the analysis showed that the presence of an electrode layer deteriorated the sensitivity.

This homebuilt isolated QCM was used for detecting human IgG (0.1-20 μ g/ml) by protein A immobilized on the one side of the 0.3-mm thick crystal. The 13th overtone resonance frequency (72 MHz) was continuously measured during injection sequences of IgG, PBS, glycine-HCL, and PBS. The kinetic analysis determined the equilibrium constant $K_A=5.21 \times 10^7$ M⁻¹. Thus, this method will drastically increase QCM sensitivity by applying to much thinner crystals.

REFERENCES

1. Sauerbrey, G. *Z. Phys.* **1959**, 155, 206-222.
2. Kanazawa, K.; Gordon, J. *Anal. Chem.* **1985**, 57, 1770-1771.
3. Martin, S.; Granstaff, V.; Frye, G. *Anal. Chem.* **1991**, 63, 2272-2281.
4. Muramatsu, H.; Dicks, M.; Tamiya, E.; Karube, I. *Anal. Chem.* **1987**, 59, 2760-2763.
5. Pan, N.; Shih, J. *Sensors and Actuators B*, **2004**, 98, 180-187.
6. Liu, Y.; Yu, X.; Zhao, R.; Shangguan, D.; Bo, Z.; Liu, G. *Biosens. Bioelectron.* **2003**, 18, 1419-1427.
7. Liu, Y.; Yu, X.; Zhao, R.; Shangguan, D.; Bo, Z.; Liu, G. *Biosens. Bioelectron.* **2003**, 19, 9-19.
8. Suri, C.; Raje, M.; Mishra, G. *Biosens. Bioelectron.* **1994**, 9, 535-542.
9. Zhou, C.; Friedt, J.; Angelova, A.; Choi, K.; Laureyn, W.; Frederix, F.; Francis, A.; Campitelli, A.; Engelborghs, Y.; Borghs, G. *Langmuir* **2004**, 20, 5857-5878.
10. Caruso, F.; Rodda, E.; Furlong, D. N.; Niikura, K.; Okahata, Y. *Anal. Chem.* **1997**, 69, 2043-2049.
11. Larsson, C.; Rodahl, M.; Hook, F. *Anal. Chem.* **2003**, 75, 5080-5087.
12. Su, X.; Robelek, R.; Wu, Y.; Wang, G.; Knoll, W. *Anal. Chem.* **2004**, 76, 489-494.
13. Stengel, G.; Hook, F.; Knoll, W. *Anal. Chem.* **2005**, 77, 3709-3714.
14. Hala'mek, J.; Makower, A.; Skla'dal, P.; Scheller, F. *Biosens. Bioelectron.* **2002**, 17, 1045-1050.
15. Ogi, H.; Ledbetter, H.; Kim, S.; Hirao M. *J. Acoust. Soc. Am.* **1999**, 106, 660-665.
16. Thompson, R. B, *Physical Acoustics*, vol 19, edited by R. N. Thurston and A. D. Pierce (Academic, New York, 1990), vol 19, p. 157.
17. Hirao, M.; Ogi, H. *EMATs for Science and Industry: Noncontacting Ultrasonic Measurements*. (Springer/Kluwer, Boston, 2003).
18. Gaerttner, M. R.; Wallace, W. D.; B. W. Maxfield. *Phys. Rev.* **1969**, 184, 702-704.
19. Ogi, H. *J. Appl. Phys.* **1997**, 82, 3940-3949.
20. Johnson, W.; Kim, S. Proc. IEEE/EIA Int. Freq. Contr. Symp. Exhib. 2000, pp. 186-190.
21. Ogi, H.; Tian, J.; Tada, T.; Hirao M. *Appl. Phys. Lett.* **2003**, 83, 464-466.
22. Ogi, H.; Hirao, M.; Tada, T.; Tian, J. *Phys. Rev. B* **2006**, 73, 174107.
23. Thompson, M.; Ballantyne, S.; Cheran, L.; Stevenson A.; Lowe C. *Analyst* **2003**, 128, 1048-1055.
24. Vasilescu, A.; Ballantyne, S.; Cheran, L.; Thompson M. *Analyst* **2005**, 130,213-220.

25. Ogi, H.; Motohisa, K.; Matsumoto, T.; Mizugaki, T.; Hirao, M. *Biosens. Bioelectron.* **2006**, 21, 2001-2005.
26. Lindmark, R.; Thorén-Tolling, K.; and Sjöquist, J. *J. Immunol. Methods* **1983**, 62, 1-13
27. Gouda, H.; Shiraishi, M.; Takahashi, H.; Kato, K.; Torigoe, H.; Arata, Y.; Shimada, I. *Biochemistry* **1998**, 37, 129-136.
28. Hanson, D.; Schumaker V. *J. Immun.* **1984**, 132, 1397-1409.
29. Ogi, H.; Fukunaga, M.; Hirao, M.; Ledbetter, H. *Phys. Rev. B* **2004**, 69, 024104.
30. Ogi, H.; Shimoike, G.; Hirao, M.; Takashima, K.; Higo, Y. *J. Appl. Phys.* **2002**, 91, 4857-4862.
31. Auld, A. *Acoustic Fields and Waves in Solids, Vol, I*, (Wiley-Interscience, New York, 1973).
32. Eddowes, M. J. *Biosensors* **1987**, 3, 1-15.
33. Guilbault, G.G.; Hock, B. **1995**, *Anal. Lett.* 28, 749-764.
34. Saha, K.; Bender, F.; Gizeli, E. *Anal. Chem.* **2003**, 75, 835-842.

Table 1. Comparison of the standardized sensitivity in the present QCM with that in the pervious studies for capturing human IgG of the concentration near 10 $\mu\text{g/mL}$. The effective area-mass density per one side is considered.

| | IgG concentration ($\mu\text{g/mL}$) | receptor | Δf (Hz) | f_1 (MHz) | $\Delta f/(nf_1)$ (10^{-6}) | sensitivity (pg/mm^2) |
|--------------------------------------|--|--------------|--------------------|----------------|------------------------------------|-------------------------------------|
| present | 10 | Protein A | 555 | 5.5 | 7.75 | 6.03 |
| Muramatsu <i>et al.</i> ⁴ | 10 | Protein A | 200 | 9 | 22 | 5.17 |
| Pan and Shih ⁵ | 10 | C60-Anti-IgG | 350 | 10 | 35 | 14.81 |
| Zhou <i>et al.</i> ⁹ | 11.5 | ODT-SAM | 18 | 5 | 3.6 | 3.05 |

Table 2. Equilibrium constant K_A , and kinetic constants k_a and k_d of IgG-sorbent binding reactions determined by acoustic methods.

| interaction system | K_A (10^7 M^{-1}) | k_a (10^4 s^{-1}) | k_d ($10^{-3} \text{ M}^{-1} \text{ s}^{-1}$) |
|---------------------------------|------------------------------------|------------------------------------|--|
| IgG-protein A (present) | 5.21 | 2.37 | 0.456 |
| IgG-protein A ³⁴ | 2.9 | 0.802 | 0.277 |
| IgG-sulfamethazine ⁷ | 0.0548 | 0.0433 | 0.792 |
| IgG-histidine ⁶ | 0.00292 | 0.0324 | 0.0011 |

FIGURE CAPTIONS

Figure 1. Piezoelectric α -TeO₂ crystal plate used for clarifying the coupling mechanism.

Figure 2. Shear-wave resonance spectra of the α -TeO₂ plate measured by the elongated spiral coil. The α -TeO₂ plate was located on the straight parts of the coil. (a)The quasistatic electric field is generated along the $\langle 110 \rangle$ direction. (b)It is generated along the $\langle 001 \rangle$ direction.

Figure 3. Shear-wave resonance spectra of the α -TeO₂ plate measured by the line antenna. The α -TeO₂ plate was located on the straight parts of the antenna. (a)The quasistatic electric field is generated along the $\langle 110 \rangle$ direction. (b)It is generated along the $\langle 001 \rangle$ direction.

Figure 4. Schematic explanation of shear strains (parallelograms) and displacements (broken lines) for (a) second-overtone and (b) third-overtone thickness resonances modes.

Figure 5. Side view and top view of the isolated electroless QCM cell. The line antenna is placed near the bottom of the cell, which radiates the quasistatic electric field to generate the shearing vibrations and receives the vibrational signals through the piezoelectric effect.

Figure 6. The flow-cell system for contactlessly measuring resonance frequencies of the isolated QCM. The received signals are processed by the superheterodyne signal processing to extract the same frequency components from the signals as the driving rf tone bursts.

Figure 7. Examples of measured resonance spectra of the AT-cut quartz plate (a) in the air and (b) in the water measured by the contactless manner. f_s , f_{qs} , and f_{ql} denote the resonance frequencies of pure shear wave, quasi shear wave, and quasi longitudinal wave, respectively. Superscript shows the overtone number. Only the pure shear wave resonances occur in the water.

Figure 8. Fractional resonance-frequency change calculated by the double-layered plate system consisting of 0.3-mm AT-cut quartz and 20-nm IgG layer. (a) Effect of the shear modulus of the IgG layer on the decrement of the resonance frequencies. (b) Relationship between the 13th-overtone

resonance frequency and the adsorbed mass of IgG with various stiffnesses of the IgG layer. Δm_f and m_{osc} are the mass of the adsorbed layer and the mass of the oscillator, respectively.

Figure 9. Calculated resonance-frequency change caused by adsorption of the 20-nm IgG layer with and without 250-nm Au electrode on the one side of the 0.3-mm AT-cut oscillator.

Figure 10. Typical response of the 13th overtone resonance frequency observed during the injection sequence. IgG, PBS, and G-HCl denote the arrival times of the IgG, PBS, and glycine-HCl buffer solutions, respectively.

Figure 11. Comparison between frequency-change behaviors after an injection of the 20 $\mu\text{g/mL}$ IgG solution for QCMs with the two surface modifications.

Figure 12. Frequency-change behaviors after injections of IgG solutions of various concentrations. Solid lines are fitted exponential curves.

Figure 13. (a) Correlation between the IgG concentration and the frequency change. (b) $1/C_{\text{IgG}}-1/\Delta f_e$ plot for determining the equilibrium constants. The solid curve denotes the fitted function of Eq. (10).

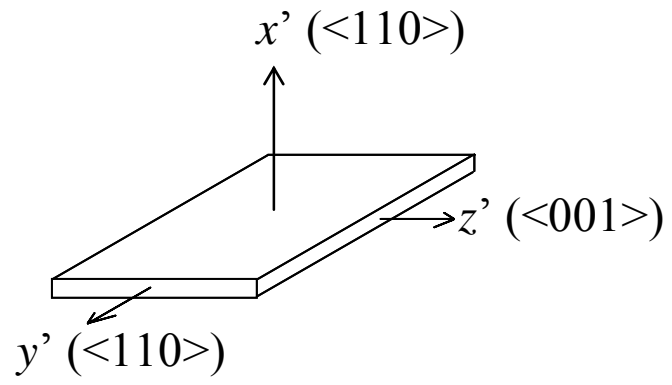


Figure 1

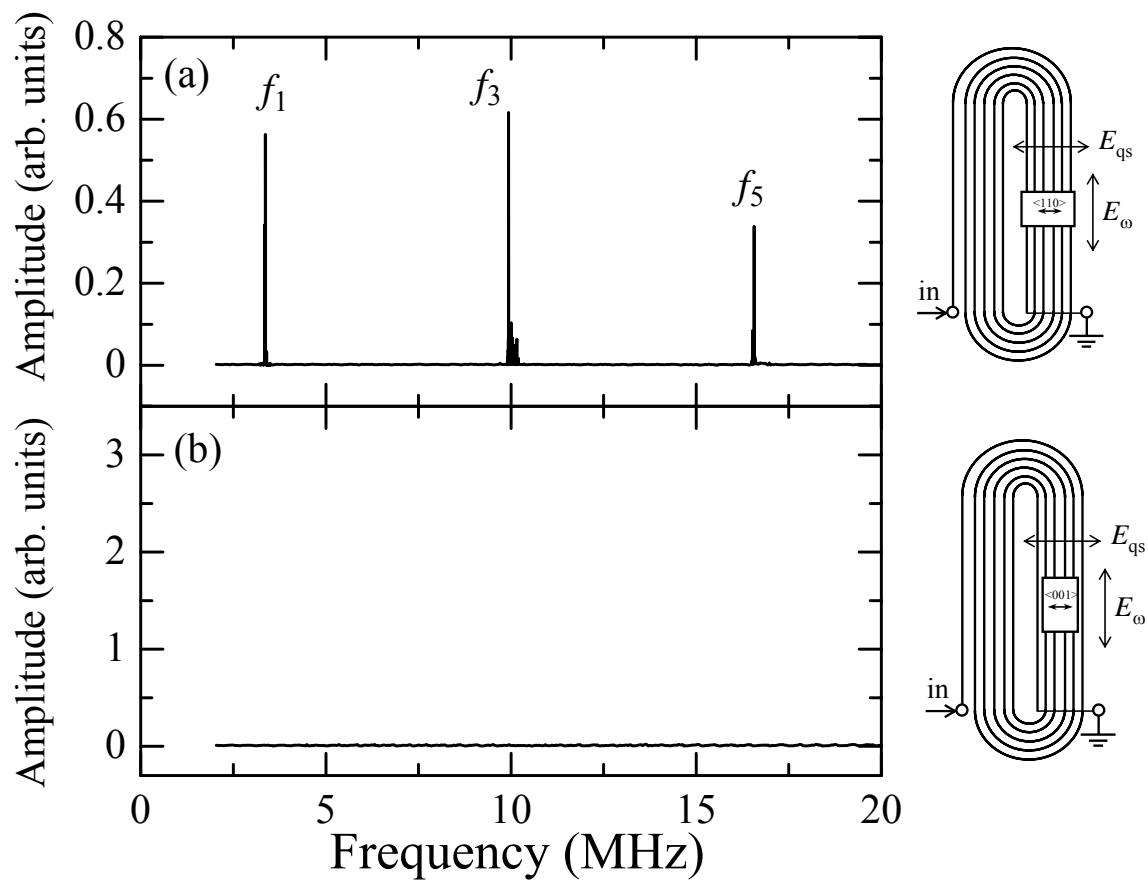


Figure 2

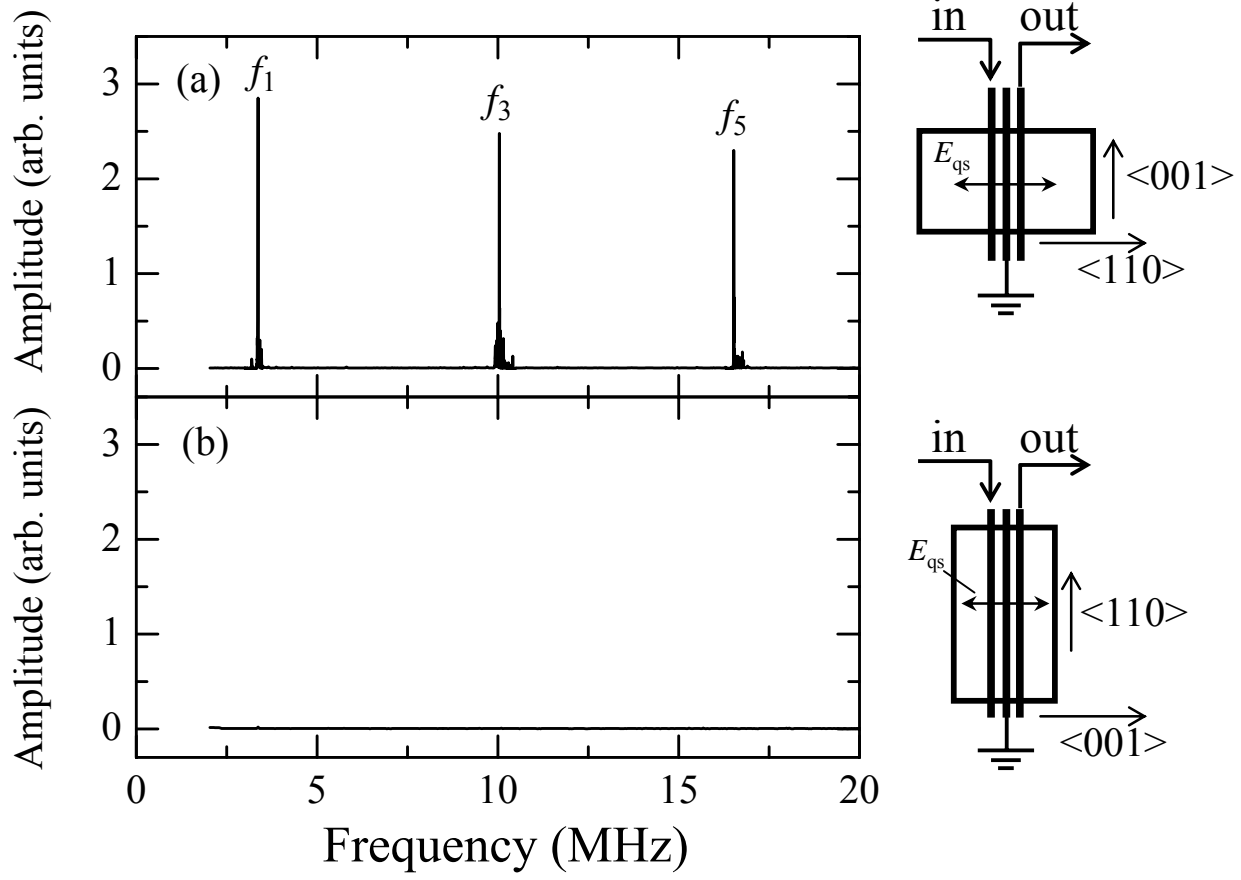


Figure 3

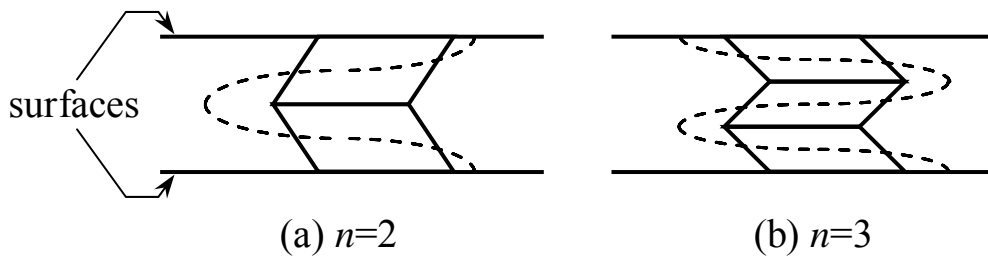


Figure 4

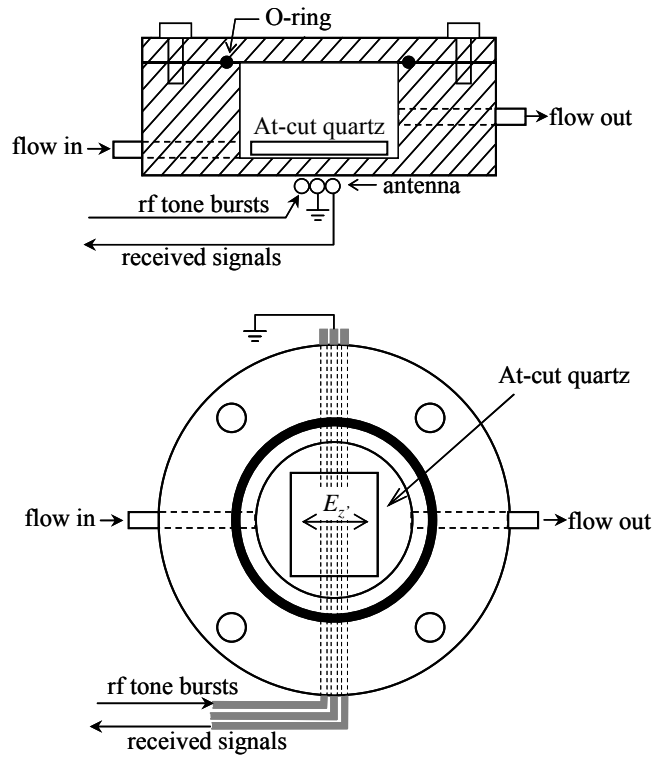


Figure 5

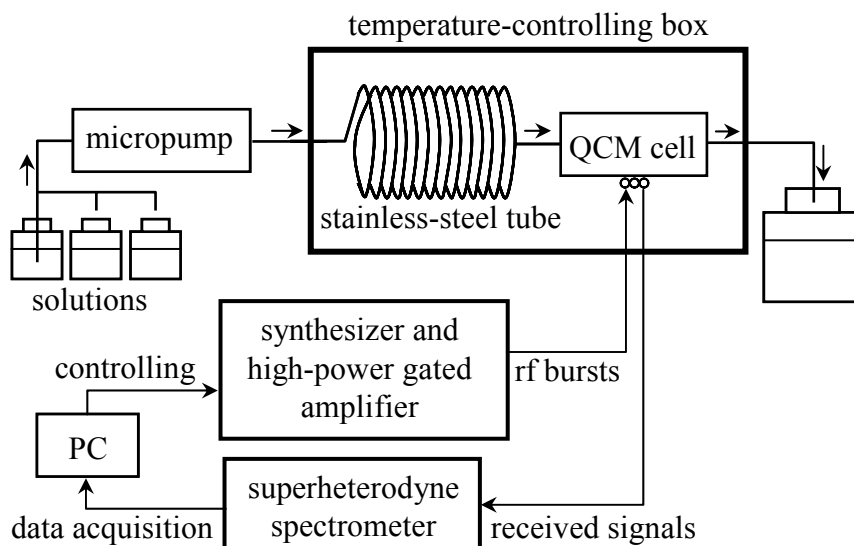


Figure 6

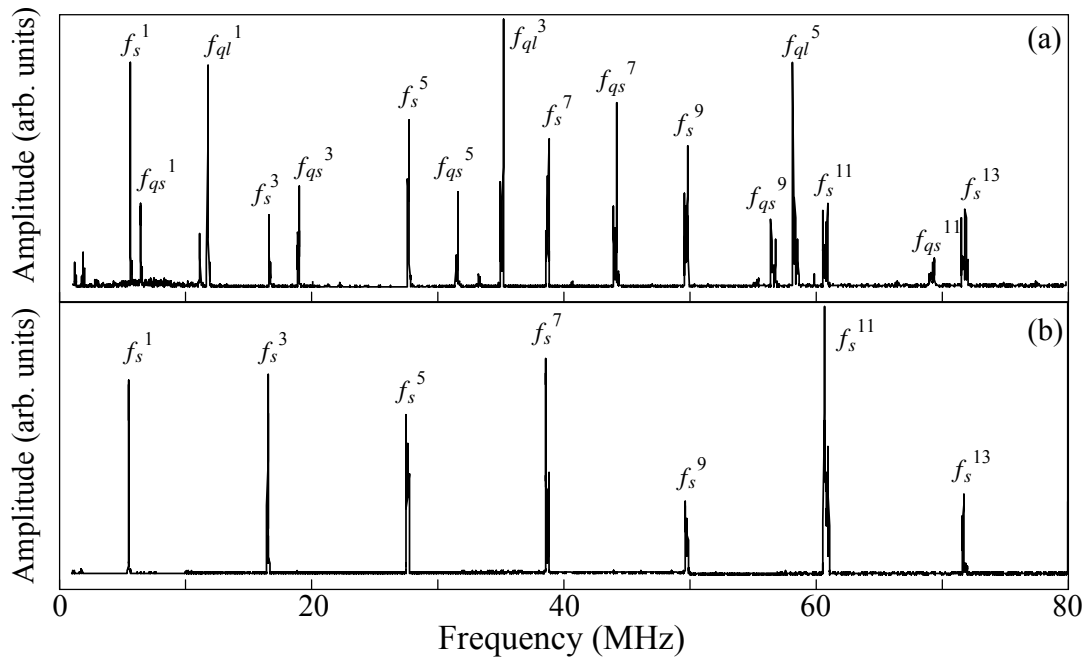


Figure 7

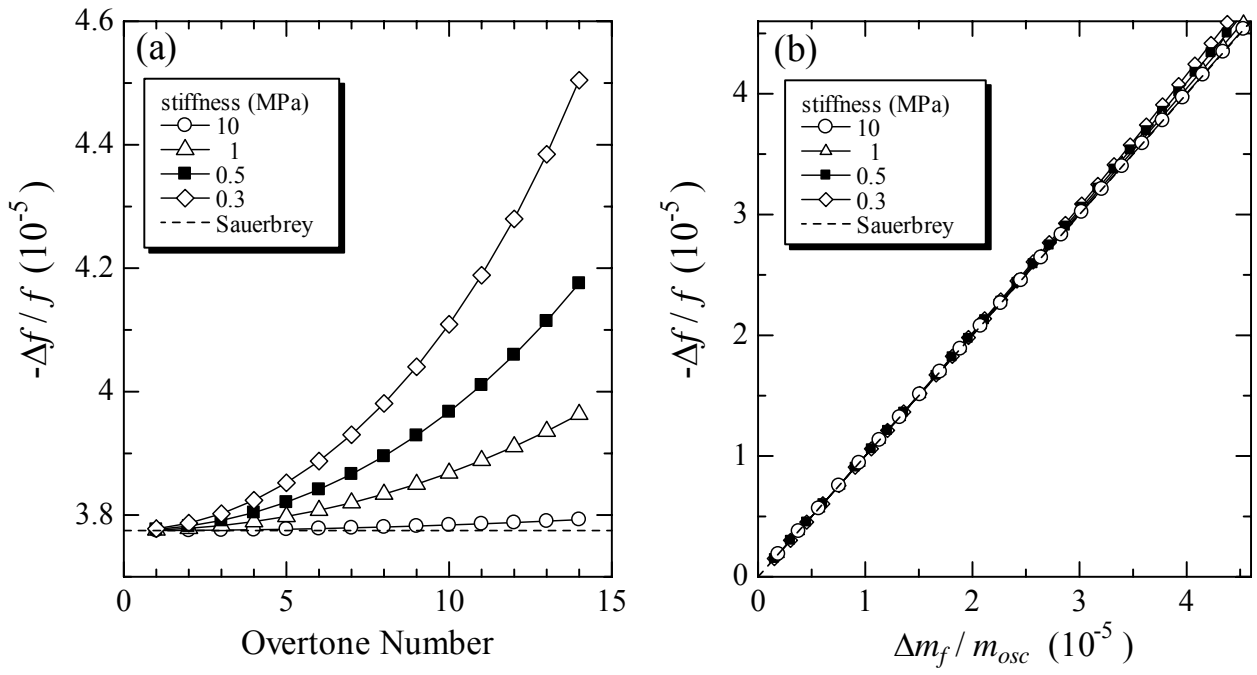


Figure 8

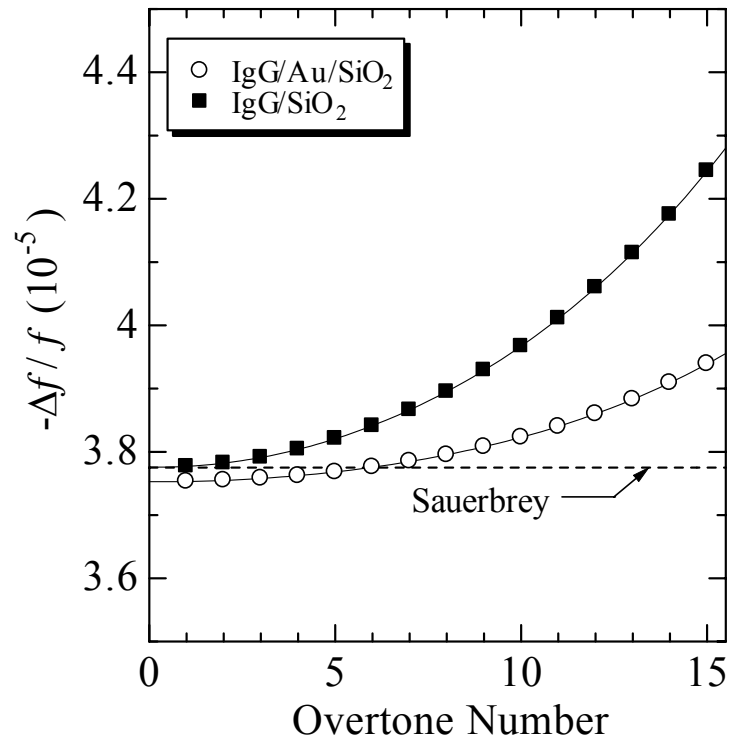


Figure 9

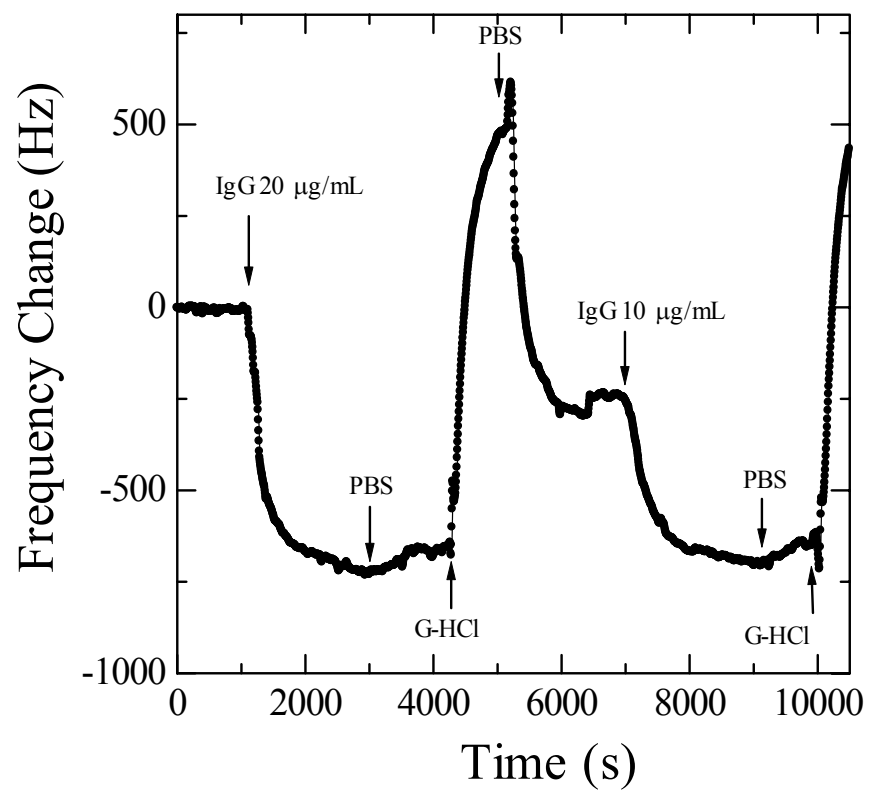


Figure 10

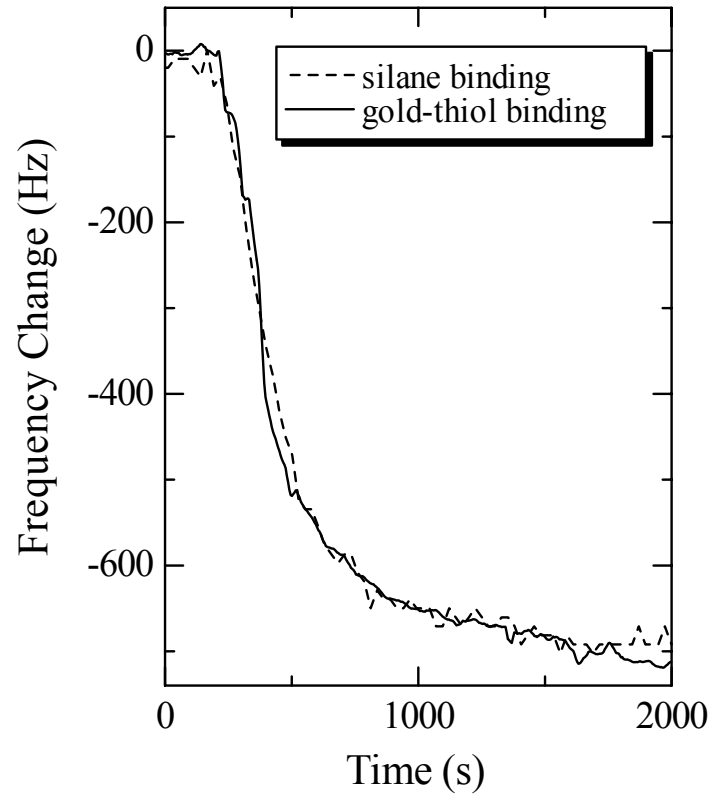


Figure 11

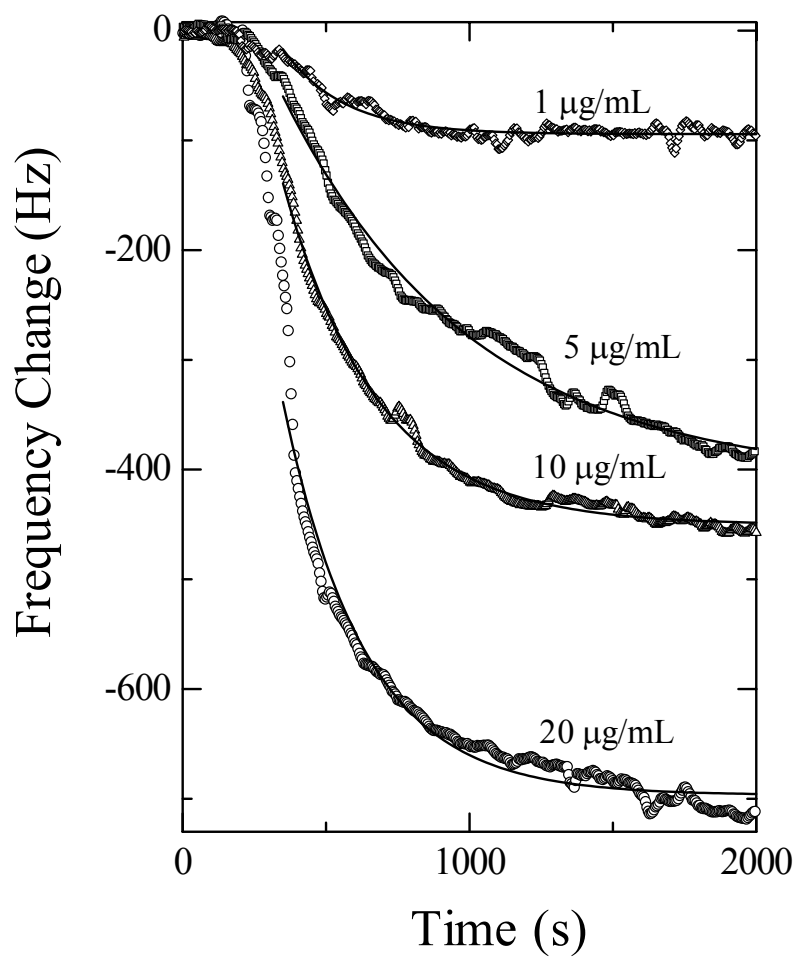


Figure 12

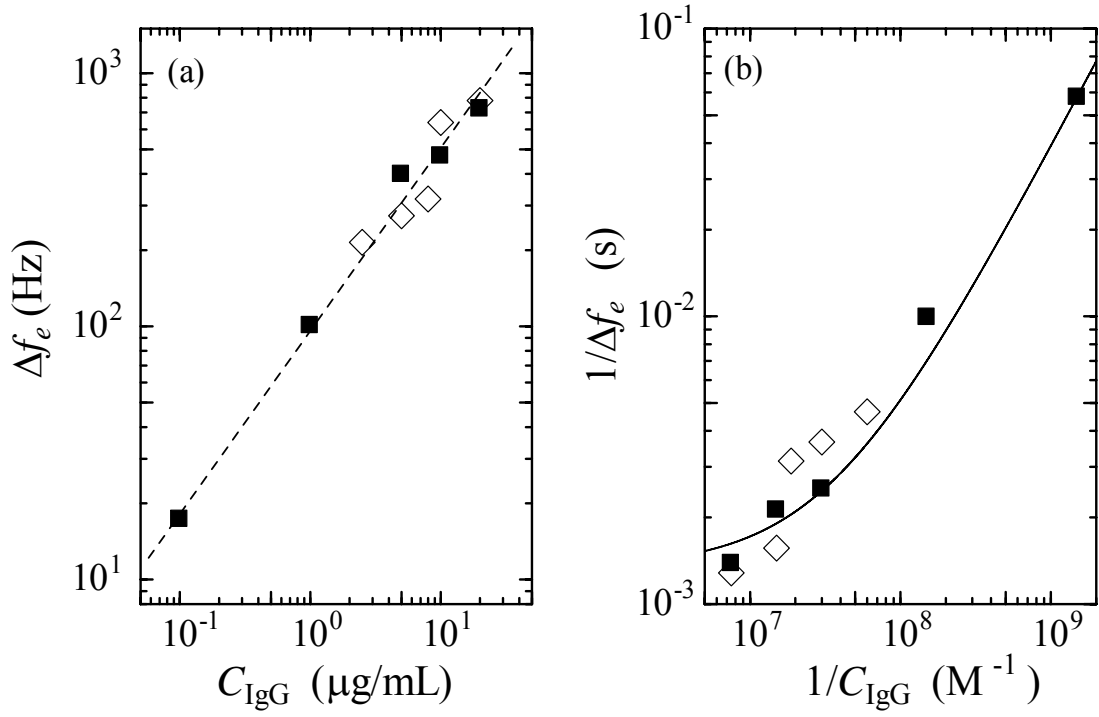


Figure 13